Breaking π–π Interactions in Carboxylic Acid Monolayers on Rutile TiO_2 (110) Leads to Unexpected Long-Range Ordering

William J. I. DeBenedetti and Melissa A. Hines*

Dept. of Chemistry and Chemical Biology, Cornell University, Ithaca NY 14853 USA

Abstract: Carboxylic acids are ubiquitous building blocks in supramolecular and surface chemistry because of their strong but reversible binding to metal cations. In these applications the relative ordering and orientation of the acids can affect performance. We present a rational approach to tuning intermolecular interactions with the goal of maintaining a favorable molecular conformation while also enabling long-range ordering. In particular, we show that scanning tunneling microscopy (STM) images of *m*- or *p*-fluorobenzoate monolayers on rutile (110) produced in aqueous solutions display very large (2 × 1) grains without the intermolecular pairing observed in similarly prepared benzoate monolayers. The lack of pairing is attributed to the electronegative fluorine substituent, which reduces π-π or quadrupolar interactions between the phenyl groups on adjacent molecules and stabilizes a favorable configuration between the aromatic head group and the carboxylate binding moiety. In spite of the reduced interactions between the head groups, the large grain sizes are indicative of intermolecular interaction energies that significantly exceed thermal energy. These strong interactions are surprising given the 6.6 Å separation between adjacent molecules. Quantitative measurements of the intermolecular interaction energies from molecularly resolved STM images are a factor of ~7 larger than those predicted by dispersion-corrected density functional theory (DFT). A number of possible origins for this discrepancy are discussed. This finding suggests a new path to the production of highly ordered monolayers and superstructures of large molecules.

Introduction

Because of their strong but reversible binding to metal cations, carboxylic acids are ubiquitous building blocks in both supramolecular and surface chemistry. For example, one of the first metal-organic frameworks (MOFs), MOF-5, consists of a cubic array of zinc oxide nuclei tethered by aromatic dicarboxylic acids, benzene-1,4-dicarboxylic acid.[1] The reversible binding of carboxylates is often credited with promoting high crystallinity in MOFs. As a second example, dye-sensitized solar cells typically use carboxylic acid linkages to attach light-absorbing, conjugated dye molecules to TiO_2 nanocrystals.[2,3] In this application, the carboxylic acid is both a tether and an electronic conduit between the molecule and the nanocrystal. Benzoic acid derivatives have also been used to control the surface dipole and modify charge injection in heterointerfaces.[4] These two fields are now coming together in the development of surface-tethered metal-organic frameworks (SURMOFs),[5–7] which use a supporting surface to enhance the stability of highly porous MOFs.

In some applications, the relative ordering and orientation of the acids can affect the properties of the structure. For example, a planar orientation of the carboxylate moiety with the aromatic π structure of organic dyes is necessary for full conjugation and good electronic hybridization with the substrate. Similarly, much of the promise of SURMOFs is based on their anticipated long-range order and high porosity, which would be well suited, for example, to ion exchange in electrovoltaic applications. The question we address is what structural motifs promote structural regularity and long-range ordering, particularly when the acids are large (*e.g.,* larger than the underlying unit cell).

As an example, benzoic acid — the simplest analogue of the dyes used in TiO_2-based dye sensitized solar cells — binds to TiO_2(110) as benzoate in two nearly isoenergetic isomers[8] as shown in Figure 1. The H atoms produced in this dissociative adsorption reaction bind to surface "bridging" O atoms, forming hydroxyls. In the "paired" isomer,[9–12] quadrupolar and dispersion interactions between adjacent aromatic head groups favor an edge-to-face orientation of the aromatic rings in which adjacent molecules tilt towards one another by 7°.[12] (The paired isomer, which has a tetrameric structure, is sometimes referred to as a

dimer due to its appearance in STM images.) This strong intermolecular interaction has the advantage of leading to long-range (2 × 1) ordering; however, it breaks the conjugation of half of the molecules to the substrate and presumably lowers the efficacy of charge transport. In contrast, the phenyl rings on the "unpaired" isomer[13,14] twist by ~20° about the surface normal to relieve steric interactions. The molecules in this isomer do not tilt, so the STM images show no molecular pairing.

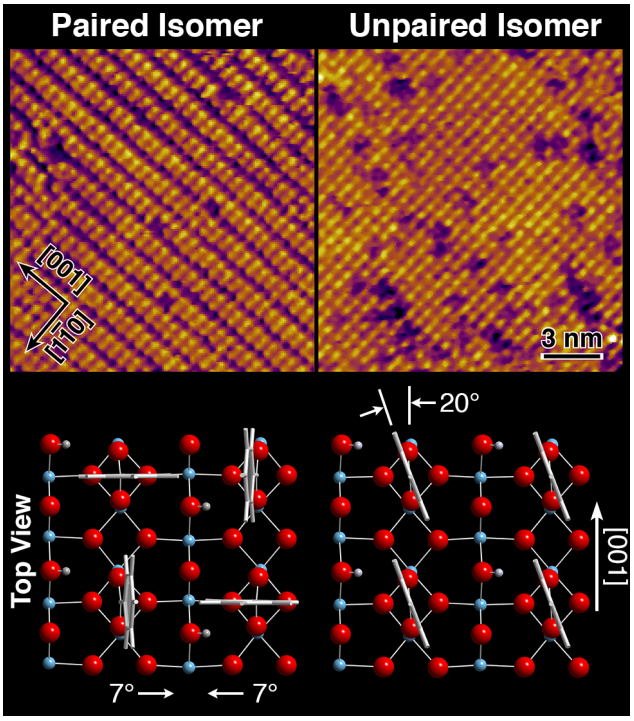

Figure 1: (Top) STM images of the "paired" and "unpaired" isomers of benzoate bound to TiO_2(110) and (bottom) molecular structures of the two isomers obtained from DFT simulations. The Ti, O, and H atoms are represented by blue, red, and white spheres, respectively. See Ref. 8 for more information.

Here, we present a rational approach to tuning intermolecular interactions with the goal of maintaining a favorable molecular conformation while also enabling long-range ordering. We show that unfavorable intermolecular interactions can be lowered by the addition of an electron-withdrawing group, such as fluorine. As suggested by the electrostatic potential maps shown in Figure 2, this chemical modification reduces edge-to-face (quadrupolar or π-π) interactions, leading to the production of monolayers with a

uniformly favorable configuration between the aromatic head group and the carboxylate binding moiety. Even though these monolayers are engineered to have reduced intermolecular interactions, they display unexpected long-range ordering, with very large adsorbate grain sizes. Quantitative measurements of the intermolecular interactions that lead to this regularity are ~8 times larger than predicted by density functional theory (DFT). This suggests a new path to the production of highly ordered monolayers and superstructures of large molecules.

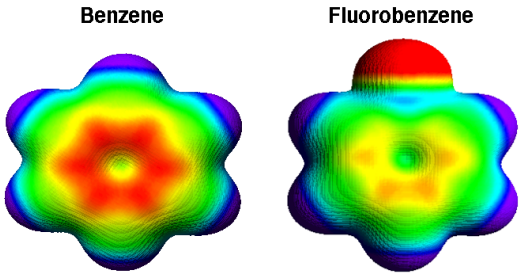

Figure 2: Electrostatic potential maps of benzene and fluorobenzene showing that the electron-withdrawing fluorine substituent reduces the quadrupolar character of the ring.

Experimental and Computational

Experimental Methods. Prior to use, rutile (110) samples were thermally reduced in ultrahigh vacuum (UHV) at 700°C for 15 min to induce sufficient conductivity for STM analysis.

Prior to use, all labware was cleaned in a 1:1:5 by volume solution of 28% NH_4OH (*aq*, EMD Millipore, ACS grade):30% H_2O_2 (*aq*, J.T. Baker, CMOS grade):ultrapure H_2O (Milli-Q) at 80ºC for 10 min then rinsed with H_2O. Rutile (110) samples were then etched in a 1:1:2 by volume NH_4OH:H_2O_2:H_2O solution at 80°C for 10 min and rinsed in H_2O to produce a clean and atomically flat surface.[15,16] This hydrophilic surface was then immersed in a room temperature, 3 mM solution of either *para*- or *meta*-fluorobenzoic acid (Sigma-Aldrich, 99%) for 10 min. Upon removal from solution, the surfaces were markedly hydrophobic and were used without rinsing. All solution processing was performed in air.

Samples were transferred to a UHV chamber through an oil-free load lock. X-ray photoemission spectroscopy (XPS) was performed on electrons collected at 70° from the surface normal after excitation

with Mg Kα x-rays,. A Tougaard baseline was removed from all spectra.[17] Small energy corrections (~0.05 eV) were applied to the reported spectra using published reference energies[18] to offset mild band bending.[19] STM images were obtained in UHV at room temperature with a W tip.

Computational Methods. Density functional theory (DFT) was used to model the structure and energetics of fluorobenzoate-terminated rutile (110) surfaces using 4 × 2 periodically repeating slabs consisting of 5 TiO_2 trilayers separated by a 12.5 Å vacuum spacing with autocompensated surfaces (Supporting Information).[20] The surface of the supercell contained 4 unsaturated Ti atoms capable of adsorbing 2 benzoate molecules at saturation. During optimization, the positions of the bottommost TiO_2 layer and its terminating bridging O rows were held fixed. Calculations were performed using DFT within the generalized gradient approximation[21] (GGA) as implemented in the Vienna *ab initio* simulation package (VASP).[22–25] Electron-ion interactions were described using the projector augmented wave (PAW) method.[26,27] Electronic states were expanded in plane waves with a kinetic energy cutoff of 400 eV and a 6 × 4 × 1 Monkhorst-Pack grid of *k* points. Brillouin-zone integration was performed using Gaussian smearing.

Both complete monolayers and isolated molecules were studied. The complete monolayers had two adsorbed molecules per unit cell. The energies of isolated molecules were calculated using 4 × 4 periodically repeating slabs with correspondingly fewer *k* points. This structure corresponds to a 1/4 saturation coverage. Representative structures are shown in the Supporting Information.

Two different functionals were used. Initial calculations were performed with the Perdew, Burke, and Ernzerhof (PBE) exchange-correlation functional.[28] When this functional led to much weaker long-range interactions than experiment, simulations were repeated using the revPBE functional,[29] which improves modeling of non-covalent interactions[35] and leads to the best overall agreement with experiment at this level of theory across a wide range of molecules.[30] For completeness, the simulations were repeated including Hubbard on-site Coulomb interactions for the Ti *d* electrons with $U = 4.1$.[31–34] All functionals were corrected for long-range dispersion interactions, as these corrections have been shown to improve the

description of noncovalent interactions and energetics across a wide range of systems.[35] Three different types of dispersion correction were used: the DFT-D3(BJ) method with Becke-Johnson damping,[36,37] the charge-density-dependent DFT-TS formulation of Tchatchenko-Scheffler,[38] and the MBD@rsSCS many-body dispersion method of Tchatchenko *et al.*[39,40]

The electrostatic potential surfaces are color maps of position-dependent electrostatic potential calculated at the PBE+D3 level and displayed on isosurfaces of constant charge density using a color scale of 1.6 V full scale with red being the most negative. The aromatic H atoms define the zero potential.

Results and Discussion

The interactions between aromatic molecules are complex,[41] involving electrostatic, dispersion, and other forces. Nevertheless, qualitative understanding can often be inferred from electrostatics. To first order, benzene, the simplest aromatic molecule, is a quadrupole with a partial negative charge above and below the plane of the ring and a partial positive charge in the plane of the ring. The addition of an electronegative atom, such as fluorine, withdraws charge from the aromatic system, thereby reducing the quadrupolar character. Based on this simple electrostatic picture, we reasoned that the addition of an electronegative substituent such as fluorine would decrease the quadrupolar interactions between adjacent adsorbed molecules, thereby destabilizing the edge-to-face isomer.

To test this hypothesis and measure the interadsorbate interactions, we used the highly site-selective etching of TiO_2(110) by basic peroxide solutions[15] to prepare rutile TiO_2 (110) surfaces with very large atomically flat terraces. Fluorobenzoate monolayers were deposited at room temperature by direct immersion of the atomically flat surfaces in aqueous solutions of either *p*- or *m*-fluorobenzoic acid. The only difference between the two isomers is the position of the fluorine atom. The para isomer leads to a monolayer in which the C-F bond is normal to the surface, whereas the meta isomer has a C–F bond nearly parallel to the surface. The use of aqueous deposition ensures that multiple adsorption/desorption events occur at every surface site during deposition. This high degree of reversibility is often cited as a key to the production of macromolecular structures with large grains, such as MOFs.

The chemical identity of the fluorobenzoate monolayers was confirmed using XPS analysis as described in the Supporting Information.

As hypothesized, the addition of a fluorine atom in either the meta or para position suppresses the formation of "paired" isomers, as shown by the STM images of *m*-fluorobenzoate monolayers in Figure 3. More surprisingly, the monolayers display a very high degree of regularity along the Ti rows, the [001] direction, and perpendicular to the Ti rows, the $[1\,\bar{1}0]$ direction. In other words, the monolayers have a near-defect-free (2 × 1) structure.

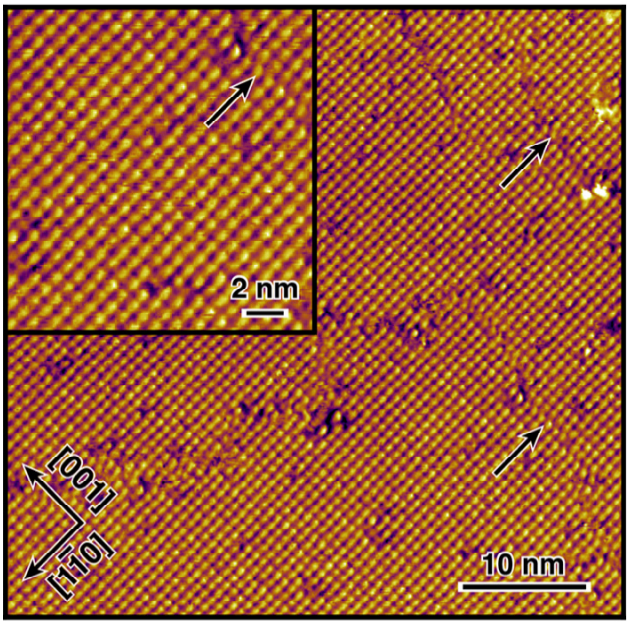

Figure 3: Low- and high-resolution STM images (50 pA, 1.5 V) of *m*-fluorobenzoate on rutile (110) show a high degree of regularity along the Ti rows, the [001] direction, and perpendicular to the Ti rows, the $[1\,\bar{1}0]$ direction, corresponding to a near-perfect (2 × 1) structure. The arrows indicate a few of the grain boundaries that disrupt perfect ordering. The scattered tall species ("white balls") are attributed to adventitious contamination.

Periodicity along the Ti rows is not surprising; this is a simple consequence of the near-complete monolayer coverage and the facile diffusivity of carboxylates along the Ti rows.[42] On the other hand, periodicity across the Ti rows is controlled by intermolecular interactions. Because of its bidentate bonding, a carboxylate can

bond to one of two interpenetrating sublattices, which we arbitrarily refer to as the “red” and “blue” sublattices. For example in the molecular model in Figure 4, the molecules on the left side are bound to the red sublattice, whereas the molecules on the right half are shifted along the Ti rows by one atom and bonded to the blue sublattice. In the model, the two domains meet at an adsorbate grain boundary that is parallel to the Ti rows, the [001] direction. To highlight the experimentally observed periodicity, regions bound to the blue and red sublattices are indicated by colored overlays in the large scale images in Figure 4.

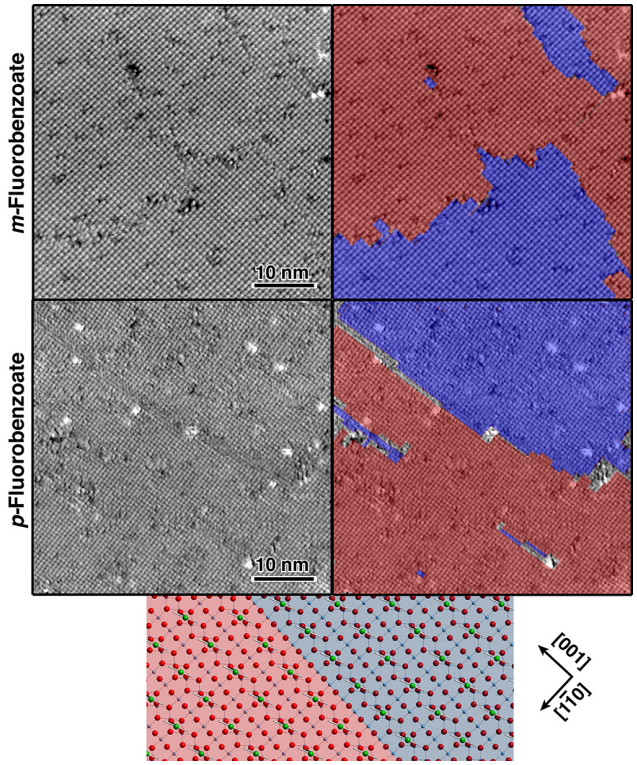

Figure 4: STM images of (top) *m*-fluorobenzoate (50 pA, 1.5 V) and (middle) *p*-fluorobenzoate monolayers (90 pA, 2.0 V) on rutile (110) with (bottom) a molecular model of an *p*-fluorobenzoate grain boundary. The images in the left and right columns are identical. The overlays on the right images indicate the two sublattices to which the molecules are bonded. The scattered tall species (“white balls”) are attributed to adventitious contamination.

In the absence of intermolecular interactions, the probability of two adjacent rows of molecules forming a grain boundary would be 50%. As a result, there would be a high density of grain boundaries, and the average width of a grain in the $[1\bar{1}0]$ direction would be two lattice constants or 13 Å.

The large size of the grain boundaries indicates the intermolecular interactions significantly exceed the thermal energy. We use a simple model to quantitatively estimate these interactions. To a first approximation, the energy of an adsorbed molecule is given by the adsorption energy of the molecule to a clean TiO_2(110) surface plus the interaction energies with its four nearest neighbors: two along the Ti rows and two across the Ti rows. In a close-packed monolayer, such as that studied here, every molecule has two nearest neighbors along the Ti row. The molecule will also have nearest neighbors across the Ti row, but these neighbors can either be on the same sublattice or the opposite sublattice. These configurations will have different energies. We assume that the adsorption energy E of a close-packed monolayer is given by

$$E = \sum_i -E_0 - \tfrac{1}{2}\gamma\left(\sigma_{i,i-\bar{a}} + \sigma_{i,i+\bar{a}}\right), \quad (1)$$

where E_0 and γ are constants, $\sigma_{i,i\pm\bar{a}}$ is 1 if the molecules ± one unit cell in the $[1\bar{1}0]$ direction are on the same sublattice as the i^{th} molecule and otherwise 0, and the sum runs over all adsorbed molecules. The constant γ is related to the adsorbate grain boundary energy. The energy E_{GB} required to create a grain boundary in an otherwise perfectly ordered $N \times N$ array of molecules is

$$E_{GB} = N\gamma\,. \quad (2)$$

As shown by the STM images in Figure 4, the adsorbate grains typically extend for many lattice sites in the [001] direction. Because of this, we assume the grains are very large in this direction and reduce the model to one dimension. Within this approximation, our model is equivalent to the one-dimensional Ising model.[43]

The probability of forming a grain boundary is related to both γ and temperature T. At very high temperatures (*i.e.,* $\gamma << kT$, where k is Boltzmann's constant), the probability P of forming a grain boundary between any two sites will be 50%. At lower temperatures, this probability will be

$$P = 0.5e^{-\gamma/kT} . \quad (3)$$

The probability of finding n grain boundaries in l molecular distances measured across the Ti rows (the $[1\,\bar{1}0]$ direction) is

$$P_{nl} = P^n(1-P)^{l-n}\frac{l!}{n!(l-n)!} . \quad (4)$$

which gives an average number of grain boundaries in l molecular distances of

$$\langle n \rangle_l = \sum_{n=0}^{\infty} nP_{nl} . \quad (5)$$

When a system is synthesized isothermally from a disordered state, such as the aqueous solution of molecules used in this experiment, the state of minimum attainable disorder (in the absence of external forces) is the thermal equilibrium state. As a result, thermodynamics and the grain boundary energy γ [*i.e.,* Equation (5)] place a lower limit on the density of grain boundaries $\langle n \rangle_l$ observable in our experiment. In other words, isothermal syntheses with slow kinetics may form monolayers with higher densities of grain boundaries than predicted by thermodynamics (*i.e.,* more disordered monolayers), but not lower densities (*i.e.,* more ordered monolayers).

Equation (5) can be used to estimate γ, the grain boundary energy, from molecularly resolved STM images. The average number of grain boundaries per 50 unit cells, $\langle n \rangle_{50}$, measured over replicate images of both isomers, was 1.24 for the meta isomer and 1.30 for the para isomer as shown in Figure 5. Because the system was synthesized at room temperature (kT = 25.7 meV), the grain boundary energies are estimated to be 3.00 kT (77 meV) and 2.96 kT (76 meV) or higher.

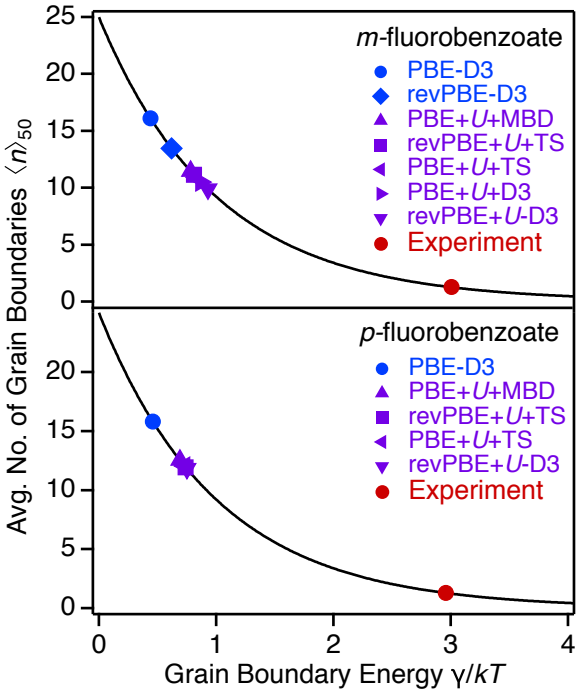

Figure 5: Estimated grain boundary energies, γ/kT, for *m*- and *p*-fluorobenzoate monolayers on rutile (110) at room temperature compared to DFT simulations using different levels of approximation. See Supplementary Information for table of results and numerical comparison.

The magnitude of the grain boundary energy is surprising given the relatively large distance between adjacent molecules of 6.6 Å. To put this energy into context, the calculated binding energy between two benzene molecules in a face-to-face orientation at this distance is 1.9 meV[44] (calculated at the MP2 level, which overestimates dispersion interactions[45]). Why is the interaction energy between benzoate molecules adsorbed to TiO_2 so much larger?

To obtain further insight, we performed DFT simulations of the structure and energetics of the monolayers. The binding of benzoic acid derivatives to TiO_2(110) is complicated by simple geometry. The distance between adjacent bidentate binding sites is 5.9 Å along the Ti rows ([001] direction), whereas the van der Waals width of benzene measured "across the flats" is ~6.5 Å. As a result, some or all of the aromatic

groups must be distorted from their preferred planar geometry to form a complete monolayer. To find the preferred geometry, we investigated a number of isomers as described in the Supplementary Information.

For both *para*- and *meta*-fluorobenzoate monolayers, the lowest energy structure had the aromatic group rotated approximately 25° about the surface normal with no "pairing," as seen in Figure 6. The *m*-fluorobenzoate monolayers were ~30 meV/molecule more stable than the corresponding *p*-fluorobenzoate monolayers, which we attribute to weak attraction between the nearest-neighbor F and H atoms on adjacent adsorbates. As discussed later, the equilibrium phenyl rotation angle balances the destabilization from increased phenyl rotation due to loss of conjugation between the aromatic group and the carboxylate with the stabilization from increased rotation due to lowered intermolecular repulsion.

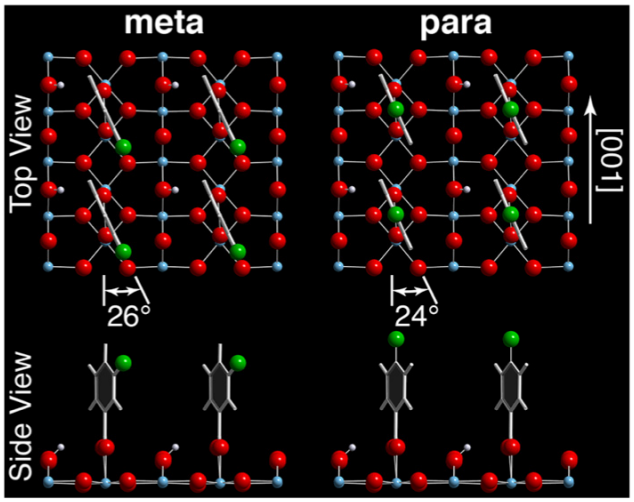

Figure 6: Molecular models of the equilibrium structure of *m*- and *p*-fluorobenzoate monolayers obtained from DFT simulations. The structural differences between the different levels of approximation are very small.

The grain boundary energy γ was estimated from DFT simulations using different levels of dispersion-corrected approximation as summarized in Figure 5 and the Supplementary Information. As described in Computational Methods, these simulations used two different functionals (PBE and revPBE), three different levels of dispersion corrections (D3, TS, and MBD@rsSCS), and were performed with and without Hubbard on-site Coulomb interactions for *d* electrons. As shown by Figure 5, all of the simulations underestimated the grain boundary energy by at least a factor of ~3, with one of the most common levels

of approximation, PBE-D3, underestimating the energy by a factor of 7. To put this into perspective, the best-performing simulations predict almost an order of magnitude more grain boundaries than experimentally observed.

To gain further insight into the intermolecular interactions, we also performed simulations of formate monolayers which have an H atom in place of the phenyl group (Supplementary Information). This replacement reduced intermolecular interactions modestly, which suggests that the long-range ordering is not primarily due to the aromatic head group. Consistent with this calculation, previous researchers have noted the surprising regularity [*i.e.,* (2 × 1) structure] of formate monolayers on rutile (110).[46,47] This same (2 × 1) structure is also observed in adventitious carboxylate monolayers formed from ppb levels of carboxylic acids in air.[48−51] Ordered carboxylic acid monolayers have been observed on TiO_2 surfaces prepared in solution[11,12] and by vapor deposition in air[48] and in ultrahigh vacuum,[46,47] which suggests that the ordering is not a consequence of exposure to air or solution. This inference is further supported by the nearly identical energetics of the *p*- and *m*-fluorobenzoate grain boundaries. Since these molecules expose different functionalities to the solution, solvent interactions would be expected to affect the two monolayers differently.

The discrepancy between experiment and simulation has many possible origins. Previous researchers have suggested that the intermolecular interaction is mediated either by the H atoms adsorbed to the bridging O rows,[46] which are invisible in STM, or long-range strain fields.[47] We simulated a number of different configurations of adsorbed H atoms; however, no significant changes in energy were found. Another possibility is that long-range dispersion interactions are only treated approximately with current DFT techniques. Recent research[52,53] has uncovered a number of systems in which these long-range interactions are substantially underestimated by current DFT methods. Finally, the Hubbard *U* parameter is itself an approximation[54] which seeks to correct over-delocalization of *d* electrons in simulations.

To be sure, more accurate DFT simulation techniques are available; however, increased accuracy comes at a substantial computational price. A recent benchmarking[30] suggests that significant improvement in

accuracy would require the use of hybrid functionals, an additional two rungs up the "Jacob's ladder" hierarchy. These functionals are prohibitively expensive for the large supercells needed for surface calculations.

Although not quantitatively accurate, DFT simulations provide insight into the role of fluorine in "breaking" the π-π interactions between neighboring adsorbates. Electrostatic potential surfaces for isolated benzoate and fluorobenzoate molecules bound to TiO_2(110) are shown in Figure 7. For all isolated molecules, the most stable bonding configuration has the plane of the aromatic ring parallel to the Ti rows ([001] direction). This geometry allows extended conjugation between the aromatic ring and the carboxylate. As a result of this extended conjugation, the quadrupolar character of the aromatic ring in the most stable bonding geometry appears to be slightly less than in the isolated molecules, which are shown in Figure 2.

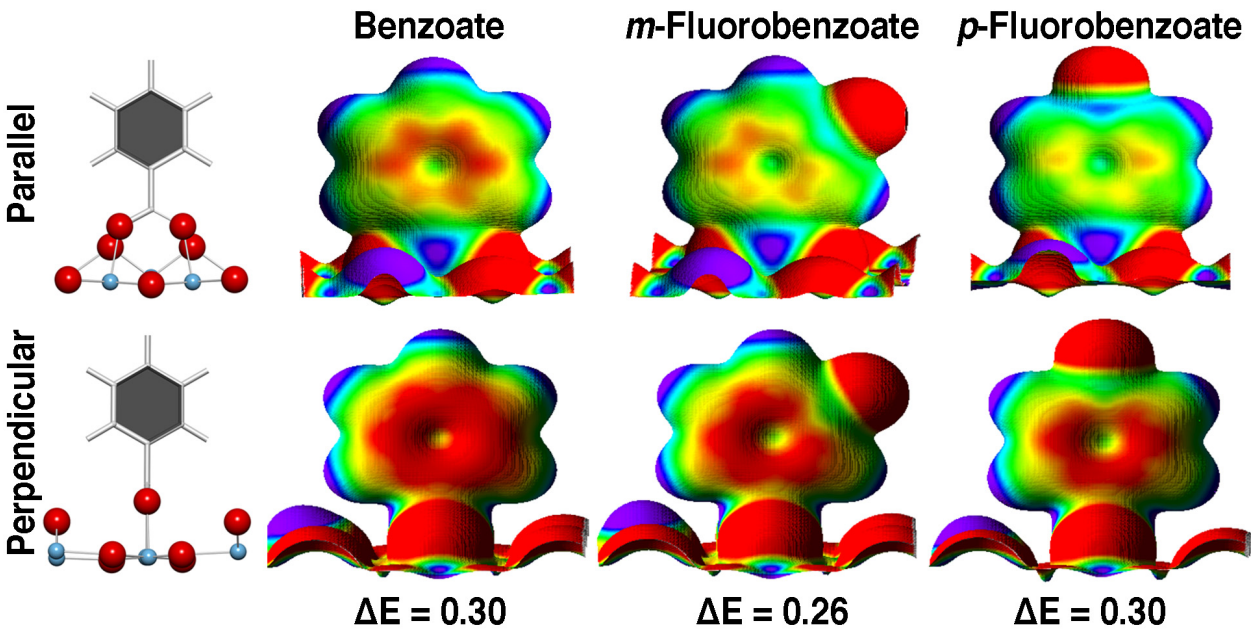

Figure 7: Electrostatic potential surfaces for isolated benzoate and fluorobenzoate molecules bound to TiO_2(110). The molecules in the top row are in their most stable bonding configuration with the plane of the aromatic ring parallel to the Ti rows. Molecules in the bottom row have their aromatic rings rotated by 90° and perpendicular to the Ti rows. The difference in energy between the two geometries, ΔE, is given below. The molecular

structure of benzoate/TiO_2(110) is shown at left for comparison. See computational methods for further description.

The formation of the "paired" benzoate/TiO_2 structure shown in Figure 1 requires a 90° rotation of half of the benzoate molecules, so we also investigated the electronic structure of isolated, similarly rotated molecules on TiO_2(110) as shown in the lower row of Figure 7. We refer to this structure as the "perpendicular" isomer. As shown by Figure 7, the perpendicular isomers were 0.25–0.30 eV less stable than the corresponding parallel isomers, which can be rationalized in terms of the broken conjugation between the aromatic ring and the carboxylate. Interestingly, the perpendicular isomer also has much more quadrupolar character than either the parallel isomer or the corresponding free molecules.

These simulations provide further insight into the chemical origins of the "paired" benzoate isomer on TiO_2(110), seen in Figure 1. This structure was originally rationalized[12] by analogy to the ground state of a square lattice of freely rotating quadrupoles, as both systems adopt a structure in which adjacent molecules or particles have an edge-to-face orientation. This analogy neglects two competing effects. On the one hand, the 90° rotation of the aromatic ring comes with a substantial energetic penalty (~10 kT at room temperature), which will destabilize the tetrameric structure. On the other hand, this rotation appears to significantly enhance the quadrupolar character of the perpendicular isomer, which should enhance the stability of the tetrameric structure. As a result, the quantitatively good agreement[12] between the predicted stabilization energy of a quadrupolar array of benzene molecules and the DFT-calculated stabilization energy of the paired benzoate/TiO_2(110) isomer may be attributed to the fortuitous cancellation of these effects.

Conclusions

STM images of *m*- or *p*-fluorobenzoate monolayers on rutile (110) produced in aqueous solutions display very large (2 × 1) grains without the intermolecular pairing observed in similarly prepared benzoate monolayers. The lack of pairing is attributed to the electronegative fluorine substituent, which reduces the π-π or quadrupolar interactions between the phenyl groups on adjacent molecules and stabilizes a favorable

configuration between the aromatic head group and the carboxylate binding moiety. In spite of the reduced interactions between the phenyl groups, the large grain sizes are indicative of strong intermolecular interaction energies that significantly exceed thermal energy. These strong interactions are surprising given the 6.6 Å separation between adjacent molecules. Quantitative measurements of the interaction energies from molecularly resolved STM images are a factor of ~7 larger than those predicted by dispersion-corrected DFT simulations. This finding suggests a new path to the production of highly ordered monolayers and superstructures of large molecules.

Author Information

Corresponding Author

Melissa.Hines@cornell.edu, +1-607-255-3040

Notes

The authors declare no competing financial interest.

Acknowledgments

This work was supported by the National Science Foundation under Award CHE-1708025 and used the National Energy Research Scientific Computing Center, a DOE Office of Science User Facility supported by the Office of Science of the U.S. Department of Energy (DE-AC02-05CH11231) as well as the Cornell Center for Materials Research Shared Facilities supported through the NSF MRSEC program (DMR-1719875).

Supporting Information Available: The Supporting Information is available free of charge on the ACS Publications website.

XPS analysis, DFT calculations of grain boundary energy, structures used in calculations.

References

[1] Rosi, N. L.; Eckert, J.; Eddaudi, M.; Vodak, D. T.; Kim, J.; O'Keeffe, M.; Yaghi, O. M. Hydrogen Storage in Microporous Metal-Organic Frameworks. *Science* **2003**, *300*, 1127-1129.

[2] Zhang, L.; Cole, J. M. Anchoring Groups for Dye-Sensitized Solar Cells. *ACS Appl. Mater. Interfaces* **2015**, *7*, 3427-3455.

[3] Hardin, B. E.; Snaith, H. J.; McGeehee, M. D. The Renaissance of Dye-Sensitized Solar Cells. *Nature Photonics* **2012**, *6*, 162-169.

[4] Krüger, J.; Bach, U.; Grätzel, M. Modification of TiO_2 Heterojunctions with Benzoic Acid Derivatives in Hybrid Molecular Solid-State Devices. *Adv. Mater.* **2000**, *12*, 447-451.

[5] Hermes, S.; Schröder, F.; Chelmowski, R.; Wöll, C.; Fischer, R. A. Selective Nucleation and Growth of Metal-Organic Open Framework Thin Films on Patterned COOH/CF_3-Terminated Self-Assembled Monolayers on Au(111). *J. Am. Chem. Soc.* **2005**, *127*, 13744-13745.

[6] Gliemann, H.; Wöll, C. Epitaxially Grown Metal-Organic Frameworks. *Materials Today* **2012**, *15*, 110-116.

[7] Heinke, L.; Gliemann, H.; Tremouilhac, P.; Wöll, C. SURMOFs: Liquid-Phase Epitaxy of Metal-Organic Frameworks on Surfaces In *The Chemistry of Metal-Organic Frameworks: Synthesis, Characterization, and Applications,* Kaskel, S., Ed.; Wiley: Weinheim **2016** pp. 523-550.

[8] DeBenedetti, W. J. I.; Skibinski, E. S.; Hinckley, J. A.; Nedessa, S. B.; Hines, M. A. Cartesian Decomposition of Infrared Spectra Reveals the Structure of Solution-Deposited, Self-Assembled Benzoate and Alkanoate Monolayers on Rutile (110). *J. Phys. Chem. C* **2016**, *120*, 24866-24876.

[9] Guo, Q.; Cocks, I.; Williams, E. M. The Adsorption of Benzoic Acid on a TiO_2(110) Surface Studied Using STM, ESDIAD, and LEED. *Surf. Sci.* **1997**, *393*, 1-11.

[10] Guo, Q.; Williams, E. M. The Effect of Adsorbate-Adsorbate Interaction on the Structure of Chemisorbed Overlayers on TiO_2(110). *Surf. Sci.* **1999**, *433-435*, 322-326.

[11] Grinter, D. C.; Woolcot, T.; Pang, C.-L.; Thornton, G. Ordered Carboxylates on TiO_2(110) Formed At Aqueous Interfaces. *J. Phys. Chem. Lett.* **2014**, *5*, 4265-4269.

[12] Skibinski, E. S.; Song, A.; DeBenedetti, W. J. I.; Ortoll-Bloch, A. G.; Hines, M. A. Solution Deposition of Self-Assembled Benzoate Monolayers on Rutile (110): Effect of π-π Interactions on Monolayer Structure. *J. Phys. Chem. C* **2016**, *120*, 11581-11589.

[13] Grinter, D. C.; Nickels, P.; Woolcot, T.; Basahel, S. N.; Obaid, A. Y.; Al-Ghamdi, A. A.; El-Mossalamy, E.-S. H.; Alyoubi, A. O.; Thornton, G. Binding of a Benzoate Dye-Molecule Analogue to Rutile Titanium Dioxide Surfaces. *J. Phys. Chem. C* **2012**, *116*, 1020-1026.

[14] Landis, E. C.; Jensen, S. C.; Phillips, K. R.; Friend, C. M. Photostability and Thermal Decomposition of Benzoic Acid on TiO_2. *J. Phys. Chem. C* **2012**, *116*, 21508-21513.

[15] Song, A.; Jing, D.; Hines, M. A. Rutile Surface Reactivity Provides Insight into the Structure-Directing Role of Peroxide in TiO_2 Polymorph Control. *J. Phys. Chem. C* **2014**, *118*, 27343-27352.

[16] Song, A.; Skibinski, E. S.; DeBenedetti, W. J. I.; Ortoll-Bloch, A. G.; Hines, M. A. Nanoscale Solvation Leads to Spontaneous Formation of a Bicarbonate Monolayer on Rutile (110) Under Ambient Conditions: Implications for CO_2 Photoreduction. *J. Phys. Chem. C* **2016**, *120*, 9326-9333.

[17] Hofmann, S. Auger- and X-ray Photoelectron Spectroscopy in Materials Science: A User-Oriented Guide; Springer: Heidelberg, 2013; pp 528.

[18] Diebold, U.; Madey, T. E. TiO_2 by XPS. *Surface Science Spectra* **1998**, *4*, 227-231.

[19] Hugenschmidt, M. B.; Gamble, L.; Campbell, C. T. The Interaction of H_2O with a TiO_2(110) Surface. *Surf. Sci.* **1994**, *302*, 329-340.

[20] Diebold, U. The Surface Science of Titanium Dioxide. *Surf. Sci. Reports* **2003**, *48*, 53-229.

[21] Kohn, W.; Sham, L. J. Self-Consistent Equations Including Exchange and Correlation Effects. *Phys. Rev.* **1965**, *140*, A1133-A1138.

[22] Kresse, G.; Hafner, J. *Ab Initio* Molecular Dynamics for Liquid Metals. *Phys. Rev. B* **1993**, *47*, 558-561.

[23] Kresse, G.; Hafner, J. *Ab Initio* Molecular-Dynamics Simulation of the Liquid-Metal-Amorphous-Semiconductor Transition in Germanium. *Phys. Rev. B* **1994**, *49*, 14251-14269.

[24] Kresse, G.; Furthmüller, J. Efficiency of *Ab-Initio* Total Energy Calculations for Metals and Semiconductors Using a Plane-Wave Basis Set. *Comput. Mat. Sci.* **1996**, *6*, 15-50.

[25] Kresse, G.; Furthmüller, J. Efficient Iterative Schemes for *Ab Initio* Total-Energy Calculations Using a Plane-Wave Basis Set. *Phys. Rev. B* **1996**, *54*, 11169-11186.

[26] Blöchl, P. E. Projector Augmented-Wave Method. *Phys. Rev. B* **1994**, *50*, 17953-17979.

[27] Kresse, G.; Joubert, D. From Ultrasoft Pseudopotentials to the Projector Augmented-Wave Method. *Phys. Rev. B* **1999**, *59*, 1758-1775.

[28] Perdew, J. P.; Burke, K.; Ernzerhof, M. Generalized Gradient Approximation Made Simple. *Phys. Rev. Lett.* **1996**, *77*, 3865-3868.

[29] Zhang, Y.; Yang, W. Comment on "Generalized Gradient Approximation Made Simple". *Phys. Rev. Lett.* **1998**, *80*, 890.

[30] Goerigk, L.; Hansen, A.; Bauer, C.; Ehrlich, S.; Najibi, A.; Grimme, S. A Look At the Density Functional Theory Zoo with the Advanced GMTKN55 Database for General Main Group Thermochemistry, Kinetics, and Noncovalent Interactions. *Phys. Chem. Chem. Phys.* **2017**, *19*, 32184-32215.

[31] Dudarev, S. L.; Botton, G. A.; Savrasov, S. Y.; Hemphreys, C. J.; Sutton, A. P. Electron-Energy-Loss Spectra and the Structural Stability of Nickel Oxide: An LSDA + *U* Study. *Phys. Rev. B* **1998**, *57*, 1505-1509.

[32] Chrétien, S.; Metiu, H. Electronic Structure of Partially Reduced Rutile TiO_2(110) Surface: Where are the Unpaired Electrons Located? *J. Phys. Chem. C* **2011**, *115*, 4696-4705.

[33] Deskins, N. A.; Rousseau, R.; Dupuis, M. Distribution of Ti^{3+} Surface States in Reduced TiO_2. *J. Phys. Chem. C* **2011,** *115*, 7562-7572.

[34] Setvin, M.; Franchini, C.; Hao, X.; Schmid, M.; Janotti, A.; Kaltak, M.; Van de Walle, C. G.; Kresse, G.; Diebold, U. Direct View of Excess Electrons in TiO_2 Rutile and Anatase. *Phys. Rev. Lett.* **2014**, *113*, 086402.

[35] Goerigk, L.; Grimme, S. A Thorough Benchmark of Density Functional Methods for General Main Group Thermochemistry, Kinetics, and Noncovalent Interactions. *Phys. Chem. Chem. Phys.* **2011**, *13*, 6670-6688.

[36] Grimme, S.; Antony, J.; Ehrlich, S.; Krieg, H. A Consistent and Accurate *Ab Initio* Parameterization of Density Functional Dispersion Correction (DFT-D) for the 94 Elements H-Pu. *J. Chem. Phys.* **2010**, *132*, 154104.

[37] Grimme, S.; Ehrlich, S.; Goerigk, L. Effect of the Damping Function in Dispersion Corrected Density Functional Theory. *J. Comput. Chem.* **2011**, *32*, 1456-1465.

[38] Tkatchenko, A.; Scheffler, M. Accurate Molecular van der Waals Interactions From Ground-State Electron Density and Free-Atom Reference Data. *Phys. Rev. Lett.* **2009**, *102*, 073005.

[39] Tkatchenko, A.; DiStasio, R. A., Jr.; Car, R.; Scheffler, M. Accurate and Efficient Method for Many-Body van der Waals Interactions. *Phys. Rev. Lett.* **2012**, *108*, 236402.

[40] Bučko, T.; Lebègue, S.; Gould, T.; Ángyán, J. G. Many-Body Dispersion Corrections for Periodic Systems: An Efficient Reciprocal Space Implementation. *J. Phys. Condens. Matter* **2016**, *28*, 045201.

[41] Martinez, C. R.; Iverson, B. L. Rethinking the Term "Pi-Stacking". *Chem. Sci.* **2012**, *3*, 2191-2201.

[42] Onishi, H.; Fukui, K.-I.; Iwasawa, Y. Molecularly Resolved Observation of Anisotropic Intermolecular Force in a Formate-Ion Monolayer on a TiO_2 (110) Surface by Scanning Tunneling Microscopy. *Colloids and Surfaces A* **1996**, *109*, 335-343.

[43] Baxter, R. J. *Exactly Solved Models in Statistical Mechanics*; Academic Press: London, **1982**; pp 486.

[44] Cacelli, I.; Cinacchi, G.; Prampolini, G.; Tani, A. Computer Simulation of Solid and Liquid Benzene with an Atomistic Interaction Potential Derived From *Ab Initio* Calculations. *J. Am. Chem. Soc.* **2004**, *126*, 14278-14286.

[45] Tkatchenko, A.; DiStasio, R. A., Jr.; Head-Gordon, M.; Scheffler, M. Dispersion-Corrected Møller-Plesset Second-Order Perturbation Theory. *J. Chem. Phys.* **2009**, *131*, 094106.

[46] Onishi, H.; Fukui, K.-I.; Iwasawa, Y. Space-Correlation Analysis of Formate Ions Adsorbed on TiO_2(110). *Jpn. J. Appl. Phys.* **1999**, *38*, 3830-3832.

[47] Yu, Y.-Y.; Gong, X.-Q. Unique Adsorption Behaviors of Carboxylic Acids at Rutile TiO_2(110). *Surf. Sci.* **2015**, *641*, 82-90.

[48] Balajka, J.; Hines, M. A.; DeBenedetti, W. J. I.; Schmid, M.; Diebold, U. High Affinity Adsorption Leads to Molecularly Ordered Interfaces on TiO_2 in Air and Solution. *Science* **2018**, *361*, 786-789.

[49] Hussain, H.; Tocci, G.; Woolcot, T.; Torrelles, X.; Pang, C. L.; Humphrey, D. S.; Yim, C. M.; Grinter, D. C.; Cabailh, G.; Bikondoa, O. *et al.* Structure of a Model TiO_2 Photocatalytic Interface. *Nature Mater.* **2017**, *16*, 461-466.

[50] Sasahara, A.; Tomitori, M. An Atomic-Scale Study of TiO_2(110) Surfaces Exposed to Humid Environments. *J. Phys. Chem. C* **2016**, *120*, 21427-21435.

[51] Serrano, G.; Bonanni, B.; Di Giovannantonio, M.; Kosmala, T.; Schmid, M.; Diebold, U.; Di Carlo, A.; Cheng, J.; VandeVondele, J.; Wandelt, K. *et al.* Molecular Ordering at the Interface Between Liquid Water and Rutile TiO_2(110). *Adv. Mater. Interfaces* **2015**, *2*, 1500246.

[52] Ambrosetti, A.; Ferri, N.; DiStasio, J., Robert A.; Tkatchenko, A. Wavelike Charge Density Fluctuations and van der Waals Interactions at the Nanoscale. *Science* **2016**, *351*, 1171-1176.

[53] Yang, Y.; Lao, K. U.; DiStasio, J., Robert A. Influence of Pore Size on the van der Waals Interaction in Two-Dimensional Molecules and Materials. *Phys. Rev. Lett.* **2019**, *122*, 026001.

[54] Kulik, H. J. Perspective: Treating Electron Over-Delocalization with the DFT + *U* Method. *J. Chem. Phys.* **2015**, *142*, 240901.

TOC Graphic